Closed-form Expressions for Fiber-Nonlinearity-Based Longitudinal Power Profile Estimation Methods

Takeo Sasai, Etsushi Yamazaki, Masanori Nakamura, and Yoshiaki Kisaka

NTT Network Innovation Laboratories, Yokosuka, Japan, takeo.sasai.cp@hco.ntt.co.jp

Abstract *Closed-form expressions for longitudinal power profile estimation methods (correlation and MMSE) are derived. Findings indicate that the spatial resolution of correlation methods is inherently limited even in noise-less and distortion-less conditions, while MMSE methods do not suffer from such limitation. ©2022 The Author(s)*

Introduction

To fully exploit the potential capacity of optical transmission systems, it is necessary to monitor the physical properties of individual link components such as fiber losses, amplifier gain tilts, and the filter passband. The recently proposed digital longitudinal monitoring [1] and optical link tomography [2] are cost-effective monitoring solutions because they reveal the component-wise characteristics from receiver-side (Rx) digital signal processing (DSP) without analog testing devices. For example, the estimations of fiber longitudinal power [1–4], the gain spectra of amplifiers [1,5], optical filter responses [1,6], and polarization-dependent loss [7], have been experimentally demonstrated.

All of these demonstrations are based on a common technique, longitudinal power profile estimation (PPE), which estimates signal power evolutions from fiber nonlinear phase rotation (NLPR). Several PPE methods have been proposed, and they can be classified into two types: correlation methods (CM) [3,8] and minimum mean square error (MMSE) methods [1,6,9]. Qualitative explanations of the performance of PPE methods have been partially provided in [1,3]. However, there has been no theoretical consideration for PPE thus far. Consequently, the fundamental performance limits of PPE (e.g., spatial resolution) as well as the pros and cons of CM and MMSE methods remain unclear. A solid theoretical foundation is indispensable to assure the reliability of PPE for practical deployment.

In this work, closed-form expressions for the longitudinal power profiles estimated by CM and MMSE are derived and compared with numerical results. The main results of this work are Eq. (8) for CM and Eqs. (11)–(13) for MMSE. Our findings indicate that (i) the spatial resolution of CM is inherently limited due to the *spatial response function* $g_{Re}(z)$ even under no noise and no distortion, while that of MMSE is not restricted by such an effect; (ii) for CM, the use of higher-baud-rate signals enables a finer spatial resolution; and (iii) CM cannot estimate the true (absolute) power, whereas MMSE can.

Model Description

Our goal is to derive the power profile estimated by CM and MMSE. Both methods obtain the signal power by estimating the nonlinear coefficients $\gamma'(z)$ in the generalized nonlinear Schrödinger equation $\frac{\partial A}{\partial z} = j\frac{\beta_2}{2}\frac{\partial^2}{\partial t^2}A - j\gamma'(z)|A|^2 A$, where $\gamma'(z) = \gamma P(z) = \gamma P(0)\exp\left(-\int_0^z \alpha(z')dz'\right)$ and $\alpha(z)$, β_2, and γ are the fiber loss, dispersion, and nonlinear constant, respectively. $P(z)$ is the optical power in fibers at distance $z \in [0, L]$. Note that normalized signals $A(z,t)$ have a constant power $P_A = 1$ during the propagation, and all the power variations due to fiber losses and amplifications are governed only by $\gamma'(z)$ [1]. Figure 1 shows the system model of the PPE we assumed. The estimation of $\gamma'(z)$, denoted by $\widetilde{\gamma}'(z_k)$, is obtained by performing correlation or MMSE between Rx signals and digitally propagated reference signals. Here, z_k ($k = 0, \dots, K-1$) denotes the measurement position. We approximate Rx signals with a sufficiently high sampling rate by using the first order regular

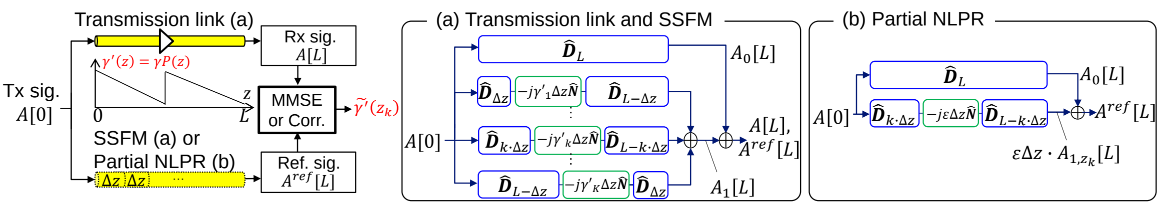

Fig. 1. Model of power profile estimation methods. In our analysis, (a) transmission link and split-step Fourier method (SSFM) and (b) partial nonlinear phase rotation (PNLPR) are modelled as first order regular perturbation.

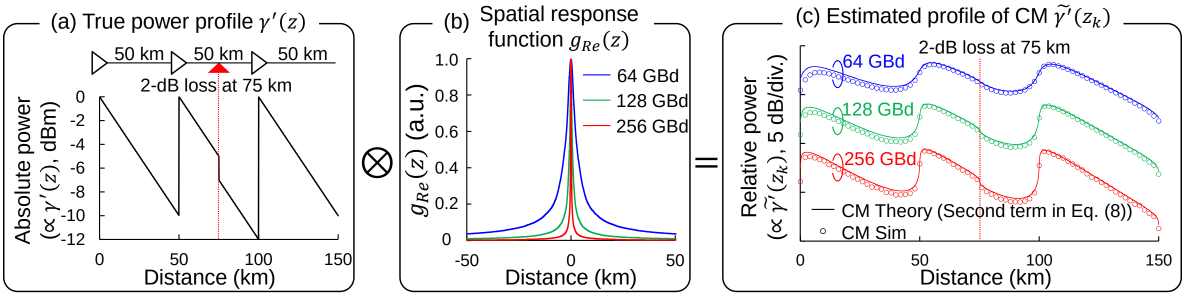

Fig. 2. Physical background of power profiles estimated by correlation method (CM) (Eq. (8)). By convolving (a) true power profile with (b) $g_{Re}(z)$, (c) CM output is obtained. In (c), derived Eq. (8) and simulation results are compared.

perturbation (RP1) [10], as (Fig. 1(a))

$$A[L,n] \simeq A_0[L,n] + A_1[L,n], \quad (1)$$

where n denotes the time sample number,

$$A_0[L,n] = \widehat{D}_{0L}\left[A[0,n]\right], \quad (2)$$

$$\begin{aligned} A_1&[L,n] \\ &= \int_0^L \gamma'(z)\left[-j\widehat{D}_{zL}\left[\widehat{N}\left[\widehat{D}_{0z}[A[0,n]]\right]\right]\right]dz \\ &\equiv \int_0^L \gamma'(z) A_{1,z}[L,n] dz, \end{aligned} \quad (3)$$

where $\widehat{D}_{zz'}[\cdot] = \mathrm{F}^{-1}\left[\exp(-j\beta_2\omega^2(z'-z)/2)\cdot \mathrm{F}[\cdot]\right]$, $\mathrm{F}[\cdot]$ is the Fourier operator and $\widehat{N}[\cdot] = |\cdot|^2(\cdot)$. In Fig. 1(a), the top path means the linear path A_0 and the other paths $A_{1,z}$ are partial nonlinear paths of which the summation forms A_1. In the following sections, the reference signals A^{ref} are also approximated by RP1, and the outputs of CM and MMSE are derived.

Correlation Methods (CM)

This section analyzes the original CM proposed by Tanimura et al. [3] and the modified one by Hahn et al. [8]. The original CM estimates $\gamma'(z)$ by correlating Rx signals and the signals with partial NLPR (PNLPR) at measurement position z_k. The latter is approximated by RP1 as

$$\begin{aligned} A^{ref}[L,n] &= \widehat{D}_{z_kL}\left[\widehat{N_e}\left[\widehat{D}_{0z_k}[A[0,n]]\right]\right] \\ &\simeq A_0[L,n] + \varepsilon\Delta z A_{1,z_k}[L,n], \end{aligned} \quad (4)$$

where $\widehat{N_e}(\cdot) = (\cdot)\exp(-j\varepsilon\Delta z|\cdot|^2) \simeq (\cdot)(1 - j\varepsilon\Delta z|\cdot|^2)$, ε is a scaling parameter for NLPR, Δz is the spatial granularity of the estimated power profiles, and $A_{1,z_k}[L,n]$ is defined in Eq. (3). The block diagram of Eq. (4) is illustrated in Fig. 1(b). Compared with Fig. 1(a), the PNLPR signals here can be understood as a part of the Rx signals with the *linear* A_0+ *single nonlinear path* A_{1,z_k}. The correlation between Rx signals A in Eq. (1) and PNLPR signals A^{ref} in Eq. (4) is expressed as

$$\begin{aligned} \rho_0[A, A^{ref}] &= \rho_0\left[A_0 + A_1, A_0 + \varepsilon\Delta z A_{1,z_k}\right] \\ &= \rho_0[A_0, A_0] + \rho_0\left[A_0, \varepsilon\Delta z A_{1,z_k}\right] \\ &\quad + \rho_0[A_1, A_0] + \rho_0\left[A_1, \varepsilon\Delta z A_{1,z_k}\right], \end{aligned} \quad (5)$$

where $\rho_m[A,B] = E\left[A^*[n]B[n+m]\right]$ is the correlation. These correlations can be simplified under the same assumption as in Gaussian noise models [11]: i.e., $A_0[z,n]$ is a stationary circular complex Gaussian process. The first term is equivalent to the power of A ($P_A = 1$), and the second and third terms vanish. The fourth term can be calculated as

$$\begin{aligned} &\rho\left(A_1, \varepsilon\Delta z A_{1,z_k}\right) \\ &= 2\varepsilon\Delta z \int_0^L \gamma'(z) g(z_k - z)\, dz \\ &= 2\varepsilon\Delta z \cdot (\gamma' \otimes_c g)(z_k), \end{aligned} \quad (6)$$

where

$$g(z) = \widehat{D}_{0z}\left[\widehat{N}\left[\widehat{D}_{z0}[\rho_m[A_0, A_0]]\right]\right]\Big|_{m=0} \quad (7)$$

and $\otimes_c$ denotes the continuous spatial convolution. Since $g(z)$ is complex-valued, taking the real part of Eq. (5) gives the estimation of $\gamma'(z)$ as

$$\tilde{\gamma}'(z_k) = P_A + 2\varepsilon\Delta z \cdot (\gamma' \otimes_c g_{Re})(z_k), \quad (8)$$

where g_{Re} is the real part of g. This is the output of CM in [3]. Equation (8) indicates that the estimated power profile is a *filtered* version of the true $\gamma'(z)$, convolved with the spatial response function $g_{Re}(z)$. This interpretation is schematically shown in Fig. 2. Since $g_{Re}(z)$ has a low-pass-filter-like characteristic (Fig. 2(b)), the output of CM has a limited spatial resolution (Fig. 2(c)). Furthermore, since $g_{Re}(z)$ scales $\gamma'(z)$, CM cannot estimate the true power. Also, Eq. (8) has an offset P_A, which hinders the estimation of the power level diagram in dB. Accordingly, Hahn et al. [8] proposed another CM to remove the offset, which uses $-j\widehat{N}$ instead of $\widehat{N_e}$ for PNLPR in Eq. (4). This corresponds to correlating Rx signals with a single nonlinear path *without* the linear path, and offset P_A consequently vanishes.

MMSE Methods

There are several different MMSE methods [1,6,9], but we here analyze the original one that uses the gradient optimization of the split-step Fourier method (SSFM) [1] or its equivalent linear least squares [9]. Both methods solve the following least squares problems:

$$\begin{aligned} \tilde{\gamma}'(z_k) &= \underset{\gamma_k'}{\operatorname{argmin}}\, I \\ &= \underset{\gamma_k'}{\operatorname{argmin}}\, E\left[|A[L,n] - A^{ref}[L,n]|^2\right]. \end{aligned} \quad (9)$$

As shown in Fig. 1(a), both Rx signals and reference signals (SSFM) are approximated by

RP1. The cost function I is then

$$\begin{aligned} I &\simeq E\left[\left|(A_0 + A_1) - \left(A_0^{ref} + A_1^{ref}\right)\right|^2\right] \\ &= E\left[\left|A_1 - A_1^{ref}\right|^2\right] \\ &= \rho_0[A_1, A_1] + \rho_0\left[A_1^{ref}, A_1^{ref}\right] \\ &\qquad - 2\Re\left[\rho_0\left[A_1, A_1^{ref}\right]\right]. \end{aligned} \tag{10}$$

From the first to the second line, we use $A_0 = A_0^{ref}$, assuming the linear part satisfies the Nyquist criterion. A_1^{ref} is the spatially discretized version of Eq. (3). These correlations can also be calculated as in Eq. (6) [11]. By calculating $\partial I / \partial \gamma'_k = 0$, we obtain

$$\begin{aligned} &\sum_{l=0}^{K-1} \widetilde{\gamma}'(z_l)\, g_{Re}(z_k - z_l)\Delta z \\ &= \int_0^L \gamma'(z) g_{Re}(z_k - z)\, dz \end{aligned} \tag{11}$$

or

$$\left(\widetilde{\gamma}' \otimes_d g_{Re}\right)(z_k) \cdot \Delta z = \left(\gamma' \otimes_c g_{Re}\right)(z_k), \tag{12}$$

where $\otimes_d$ denotes the discrete spatial convolution. This *discrete vs. continuous* convolution equation gives us an intuitive understanding of the spatial resolution of the MMSE methods. As the spatial step size Δz becomes finer, the discrete convolution in Eq. (11) approaches the continuous one on the right-hand side, which implies $\widetilde{\gamma}'(z_k)$ approaches the true $\gamma'(z)$. Thus, the spatial resolution of MMSE is not as limited by g_{Re} as that of CM, and MMSE can estimate the true power. The estimated profile is obtained by deconvolving g_{Re} as

$$\widetilde{\gamma}'(z_k) = \frac{1}{\Delta z} \cdot \mathrm{F}^{-1}\left[\frac{\mathrm{F}\left[\left(\gamma' \otimes_c g_{Re}\right)(z_k)\right]}{\mathrm{F}\left[g_{Re}(z_k)\right]}\right]. \tag{13}$$

This is the output of the MMSE methods. A matrix form of Eq. (13) using linear least squares can be found in [9].

Verification of Analytical Results

First, we conducted numerical simulations (Fig. 2(c)) to verify the analytical results of CM. The signals were probabilistically shaped (PS) 64QAM with an entropy of 4.347 bits and a roll-off factor of 0.1. The tested link was 50 km × 3-span with a 2-dB loss inserted at 75 km, and the fiber launch power was 0 dBm. No noise was added so as to investigate the performance limit. The fiber propagation was emulated by SSFM with a spatial step size of 25 m and an over-sampling rate of 20 samples/symbol. The fiber parameters were α = 0.20 dB/km, β_2 = –20.6 ps^2/km, and γ = 1.30 W^{-1}km^{-1}. The spatial granularity for the estimation was Δz = 2 km. Hahn's CM [8] was used for the numerical simulation of CM (circles). We observe that the power profiles predicted by Eq. (8) are in good agreement with the numerical results. The slight deviation near the Tx side is due to the fact that

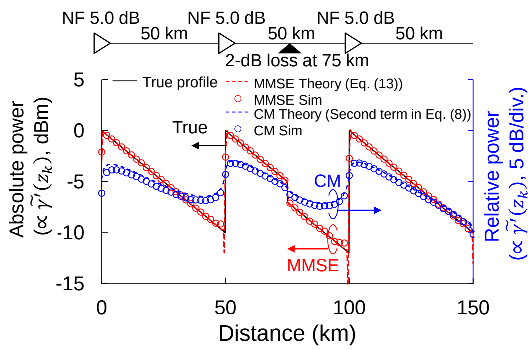

Fig. 3. Comparison of derived equations (Eq. (8) for CM and Eq. (13) for MMSE), simulation results, and true profile. Since CM does not estimate true power, a different axis is used.

the Tx signals (PS-64QAM) used in the simulation differ from the Gaussian distribution. As mentioned, the spatial resolution of CM is limited due to $g_{Re}(z)$, even under no noise and no distortion. However, as the baud rate increases, $g_{Re}(z)$ becomes more delta-function-like due to a more chromatic dispersion effect, which results in sharper power profiles and enhanced spatial resolution. This finding matches the results in [3], where the position of an anomaly loss was identified more precisely with higher-baud-rate signals.

Next, we compared the analytical results of MMSE and the numerical results (Fig. 3). In this evaluation, the tested baud rate was fixed to 128 GBd, and the noise figures of the amplifiers were set to 5.0 dB. Δz was set to 0.5 km but decimated to 2 km when plotting profiles. The linear least squares method [9] was used for the numerical simulation of MMSE. We observe that, for MMSE, the theoretical line (Eq. (13)) precisely predicts the power profile obtained by simulation. Note that, since CM does not estimate the true power, the second vertical axis is used for CM profiles. Furthermore, MMSE shows an excellent agreement with the true power profile, while CM significantly deviates from it. These deviations of CM originate from the convolution with $g_{Re}(z)$.

Conclusions

We have derived closed-form expressions for PPE methods (CM and MMSE) and confirmed their agreement with numerical simulations. The derived Eq. (8) indicates that the power profile estimated by CM is the convolution of the true power profile $\gamma'(z)$ and the spatial response function $g_{Re}(z)$, and thus the spatial resolution is limited even under no noise and no distortion. In contrast, Eqs. (11)–(13) indicate that the power profile estimated by MMSE approaches the true power profile under $\Delta z \to 0$ and offers a sufficiently high spatial resolution.

References

[1] T. Sasai, M. Nakamura, E. Yamazaki, S. Yamamoto, H. Nishizawa, and Y. Kisaka, “Digital longitudinal monitoring of optical fiber communication link,” *Journal of Lightwave Technology*, vol. 40, no. 8, pp. 2390–2408, 2022. DOI: 10.1109/JLT.2021.3139167.

[2] T. Tanimura, S. Yoshida, K. Tajima, S. Oda, and T. Hoshida, “Concept and implementation study of advanced DSP-based fiber-longitudinal optical power profile monitoring toward optical network tomography,” *Journal of Optical Communications and Networking*, vol. 13, no. 10, PPE132-E141, 2021. DOI: 10.1364/JOCN.425494.

[3] T. Tanimura, S. Yoshida, K. Tajima, S. Oda, and T. Hoshida, “Fiber-longitudinal anomaly position identification over multi-span transmission link out of receiver-end signals,” *Journal of Lightwave Technology*, vol. 38, no. 9, pp. 2726–2733, 2020. DOI: 10.1109/JLT.2020.2984270.

[4] A. May, F. Boitier, E. Awwad, P. Ramantanis, M. Lonardi, and P. Ciblat, “Receiver-based experimental estimation of power losses in optical networks,” *IEEE Photonics Technology Letters*, vol. 33, no. 22, pp. 1238–1241, 2021. DOI: 10.1109/LPT.2021.3115627.

[5] M. R. Sena, R. Emmerich, B. Shariati, J. K. Fischer, and R. Freund, “Link Tomography for Amplifier Gain Profile Estimation and Failure Detection in C+L-band Open Line Systems,” *Optical Fiber Communications Conference and Exhibition (OFC)*, Th1H.1, 2022.

[6] S. Gleb, P. Konstantin, J. Luo, and B. Zheng, “Fiber link anomaly detection and estimation based on signal nonlinearity,” *European Conference on Optical Communication (ECOC)*, Tu2C2.5, 2021. DOI: 10.1109/ECOC52684.2021.9606094.

[7] M. Eto, K. Tajima, S. Yoshida, S. Oda, and T. Hoshida, “Location-resolved PDL monitoring with Rx-side digital signal processing in multi-span optical transmission system,” *Optical Fiber Communications Conference and Exhibition (OFC)*, Th1C.2, 2022.

[8] C. Hahn, J. Chang, and Z. Jiang, “Localization of reflection Induced multi-path-interference over multi-span transmission link by receiver-side digital signal processing,” *Optical Fiber Communications Conference and Exhibition (OFC)*, Th1C.3, 2022.

[9] T. Sasai, E. Yamazaki, M. Nakamura, and Y. Kisaka, “Proposal of linear least squares for fiber-nonlinearity-based longitudinal power monitoring in multi-span link,” OptElectronics and Communications Conference/ International Conference on Photonics in Switching and Computing (OECC/PSC), 2022.

[10] A. Vannucci, P. Serena, and A. Bononi, “The RP method: A new tool for the iterative solution of the nonlinear Schrodinger equation,” *Journal of Lightwave Technology*, vol. 20, no. 7, pp. 1102–1112, 2002. DOI: 10.1109/JLT.2002.800376.

[11] P. Serena and A. Bononi, “An alternative approach to the Gaussian noise model and its system implications,” *Journal of Lightwave Technology*, vol. 31, no. 22, pp. 3489–3499, 2013. DOI: 10.1109/JLT.2013.2284499.